ISSN: 2472-3703 DOI: 10.6911/WSRJ.202506_11(6).0010

Investigating Methyl Substitution Position Effect on the ESIPT Process in 2-(2'-Hydroxyphenyl) Benzothiazole Derivatives

Yilong Wang[1], You Li[1,*], Dongxiang Li[1]

[1]College of Science, Heilongjiang University of Science and Technology, Harbin 150022, Heilongjiang, China

[*]Corresponding author email: liyou@usth.edu.cn

Abstract

Substituent position significantly influences the excited-state intramolecular proton transfer (ESIPT) behavior of 2-(2-hydroxyphenyl)-benzothiazole (HBT) derivatives, which are widely applied in fluorescent sensing. This study compares o-HBT-H and m-HBT-H to explore methyl substitution effects on ESIPT. Using by density-functional theory (DFT) and time-dependent DFT methods, optimized geometries calculations reveal that m-HBT-H exhibits stronger intramolecular hydrogen bonding in S_1 state, enhancing ESIPT activity. Electrostatic potential and frontier molecular orbitals FMOs analyses confirm methyl substitution modulates charge redistribution, strengthening intramolecular interactions. Infrared (IR) spectra and potential energy curves further validate the better ESIPT performance for m-HBT-H. These results provide a theoretical basis for designing advanced HBT-based fluorescent probes with tailored ESIPT properties.

Keywords

Hydrogen bond, DFT/TDDFT, HBT derivatives, ESIPT.

1. INTRODUCTION

In rapidly evolving field of fluorescence sensing, 2-(2-hydroxyphenyl)-benzothiazole (HBT) derivatives have emerged as a class of compounds with remarkable photochemical and photophysical properties, making them highly valuable for the development of advanced fluorescent probes [1-3]. These derivatives are particularly noted for their ability to undergo excited-state intramolecular proton transfer (ESIPT). The mechanism has been widely recognized for its potential to enhance selectivity [4], sensitivity [5] of fluorescent sensors. ESIPT involves transfer of a proton within molecule upon excitation, leading to large Stokes shift in ground (S_0) and excited (S_1) states [6, 7]. This unique property not only enriches molecular luminescence characteristics but also offers a powerful tool for designing ratiometric fluorescent sensors. These sensors are highly valued for their ability to reduce environmental interferences and enable quantitative analysis.

Zhao et al. [8] recently reported a fluorescent probe o-HBT-H based on HBT backbone. The fluorescent probe, strategically functionalized with cyano groups to reinforce molecular planar rigidity and substituted with para-methyl moieties, exhibited remarkable selectivity toward Cu^{2+} detection. The study also proposed that methyl substitution position in o-HBT-H might modulate ESIPT process through steric or electronic effects. However, this hypothesis remains unverified, presenting a gap in our understanding of relationship between substituent position and photophysical properties in HBT derivatives.

ISSN: 2472-3703 DOI: 10.6911/WSRJ.202506_11(6).0010

The spatial distribution of substituents and their inherent electronic effects are critical factors that influence photophysical properties for HBT derivatives. To further explore this relationship and provide a comprehensive understanding of how methyl substitution position affects ESIPT mechanism, this study employs o-HBT-H as a parent molecule. By altering methyl substitution position on benzene ring, we construct m-HBT-H and utilize theoretical calculations to systematically investigate influence of methyl position on ESIPT process (Fig. 1). This work aims to expand design dimensions of ESIPT probes, providing a theoretical foundation for development of next-generation fluorescent sensors with high sensitivity, selectivity, and environmental adaptability.

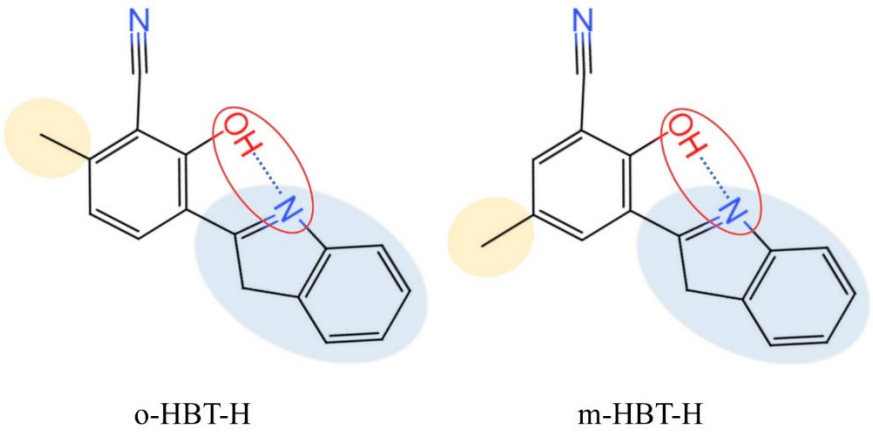

Figure 1. Chemical structures of o-HBT-H, m-HBT-H

2. METHOD

All calculations presented herein have been conducted utilising Gaussian 16 program [9]. The geometrical configurations of o-HBT-H and m-HBT-H in S_0 and S_1 states were optimised using DFT and TDDFT methods, as well as B3LYP functional and TZVP basis set, respectively [10-12]. The integral equation formalism for polarizable continuum model was employed to simulate effect of THF solvent on molecular system. No atoms were bound during structure optimization process for S_0 and S_1 states. Subsequent to structure optimisation, calculations were made of bond lengths, electrostatic potentials, frontier molecular orbitals (FMOs) and infrared (IR) vibrational spectra for two molecules in S_0 and S_1 states. A non-covalent interaction analysis was conducted utilising Multiwfn program [13, 14], with subsequent visualisation performed through utilisation of Gnuplot and VMD software [15]. In addition, potential energy curves for two compounds in S_0 and S_1 states were obtained by gradually extending O_1-H_1 bond length in steps of 0.05 Å. The potential energy curves of the compounds in S_0 and S_1 states were scanned to visualize the proton transfer process of the compounds.

3. RESULTS AND DISCUSSION

3.1. Optimized geometries analysis

The optimised o-HBT-H and m-HBT-H geometries are demonstrated in Fig. 2. Critical structural parameters such as O_1-H_1 bond, H_1...N_1 bond lengths and dihedral angle angles related to intramolecular hydrogen bond are shown in Table 1. After excitation of o-HBT-H, O_1-H_1 bond length shifts from 1.000 Å in S_0 state to 1.023 Å in S_1 state, while H_1...N_1 bond length shifts from 1.699 Å in S_0 state to 1.614 Å in S_1 state. Besides, for m-HBT-H, bond lengths of O_1-H_1 and H_1...N_1 change from 0.999 Å and 1.703 Å in S_0 state to 1.047 Å and 1.545 Å in S_1 state respectively. In contrast to S_0 state, for both o-HBT-H and m-HBT-H molecules in S_1 state, O_1-H_1

ISSN: 2472-3703 DOI: 10.6911/WSRJ.202506_11(6).0010

bond lengthens and H_1...N_1 bond shortens. This indicates that hydrogen bond interaction within o-HBT-H and m-HBT-H molecules is enhanced from S_0 state to S_1 state.

o-HBT-H excitation from S_0 state to S_1 state, dihedral angles C_1-C_2-C_3-H_1 as well as N_1-C_5-C_6-C_7 angles are almost constant. For m-HBT-H, from S_0 state to S_1 state, dihedral angles N_1-C_5-C_6-C_7 remain largely constant, while C_2-C_8-C_3-H_1 angles undergo a shift from -165.8° to -145.5°. Compared with S_0 state, dihedral angle C_2-C_8-C_3-H_1 for m-HBT-H in S_1 state undergoes a change. These results strongly suggest that intramolecular group of m-HBT-H underwent twisting in S_1 state.

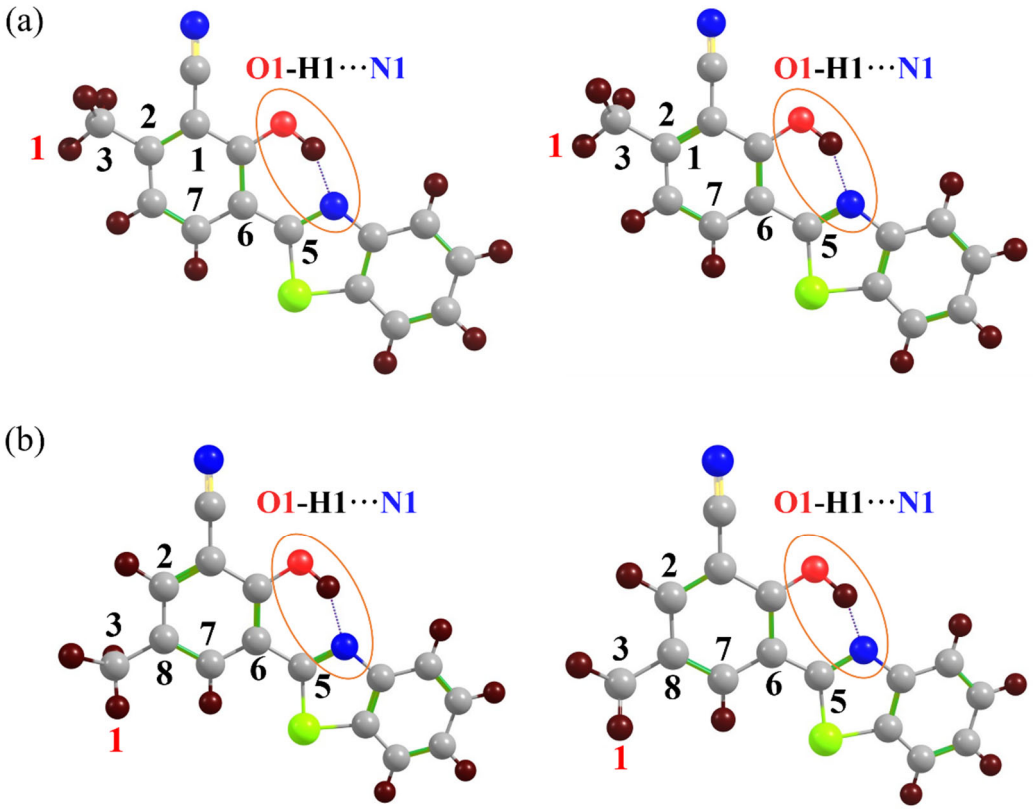

Figure 2. Molecular configurations of o-HBT-H (a), m-HBT-H (b) in S_0 (left), S_1 (right) state

Table 1. Significant bond lengths (Å) and dihedral angles (°) of o-HBT-H and m-HBT-H in S_0 and S_1 state

		O_1-H_1	H_1...N_1	C_1-C_2-C_3-H_1	N_1-C_5-C_6-C_7	C_2-C_8-C_3-H_1
o-HBT-H	S_0	1.000	1.699	-180.0	-180.0	-
	S_1	1.023	1.614	-180.0	-180.0	
m-HBT-H	S_0	0.999	1.703	-	-180.0	-165.8
	S_1	1.047	1.545		-179.8	-145.5

3.2. Electrostatic potential analysis

Electrostatic potential analysis has been demonstrated to reveal charge distribution within molecule, thereby facilitating understanding of charge transfer for molecule in excited state. The electrostatic potential distribution shown in Fig. 3 reveals electrostatic potential differences between o-HBT-H and m-HBT-H using a colour gradient. In figure, blue indicates

ISSN: 2472-3703 DOI: 10.6911/WSRJ.202506_11(6).0010

negative potential, red represents positive potential, white corresponds to near-zero potential, green spheres mark minima, and yellow spheres show maxima.

For o-HBT-H, O_1 electrostatic potential (blue region) is -42.74 kcal/mol, N1 electrostatic potential (red region) is 11.53 kcal/mol. O_1 electrostatic potential of m-HBT-H is -42.51 kcal/mol, and electrostatic potential of N_1 is 11.98 kcal/mol. Electrostatic potential analysis demonstrates that electrostatic potential difference of m-HBT-H is greater than o-HBT-H, indicating that its molecular surface charge polarization is more pronounced. Furthermore, O_1 negative potential of m-HBT-H is lower compared to o-HBT-H and less constraints on H_1.

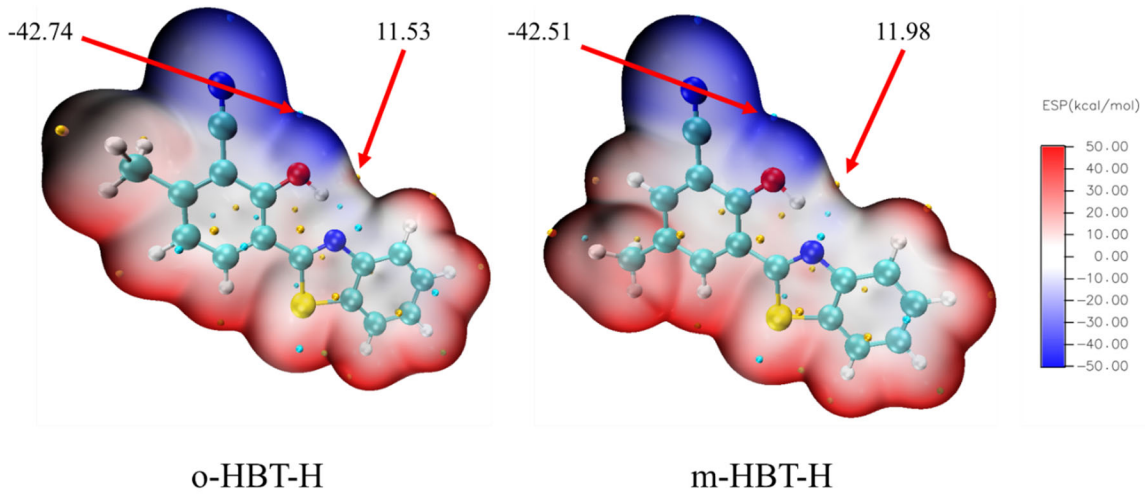

Figure 3. Electrostatic potential Distribution for o-HBT-H, m-HBT-H

3.3. FMOs analysis

In order to explore intramolecular charge distribution, we calculated FMOs of o-HBT-H and m-HBT-H. As shown in Table 2, orbital leaps from HOMO excitation to LUMO of two molecules from S_0 state to S_1 state contributed 96.2% and 97.4%, respectively, indicating that two molecules mainly corresponded to leaps between the HOMO and LUMO. Therefore, we calculated HOMO and LUMO for o-HBT-H and m-HBT-H, as shown in Fig. 4.

From HOMO to LUMO, both molecules show a decrease in electron density on proton donor O_1 and an increase in electron density on proton acceptor N_1. The results demonstrated that redistribution of electron density during excitation can facilitate intramolecular proton transfer from O_1 to N_1. o-HBT-H and m-HBT-H have Mulliken charges for O_1 and N_1 listed in Table 3. For o-HBT-H, charge of O_1 decreased from -0.266 a.u. to -0.261 a.u. during excitation, while charge of N1 increased from -0.125 a.u. to -0.135 a.u.. In contrast, O_1 charge of m-HBT-H decreased from -0.270 a.u. to -0.268 a.u., while N_1 charge increased from -0.127 a.u. to -0.132 a.u. The decrease in O_1 charge and increase in N_1 charge indicate that electron density redistribution during excitation promotes H_1 transfer from O_1 donor to N_1 acceptor in o-HBT-H and m-HBT-H. Calculations of FMOs show that charge redistribution during excitation enhances intramolecular hydrogen bond strength. During transfer process, m-HBT-H transfers more electrons to O_1 atom and binds less to H_1 atom compared to o-HBT-H, and interaction between N_1 and H_1 atoms will be stronger. The results indicate that intramolecular hydrogen bond interaction is stronger in m-HBT-H. FMOs analysis shows that intramolecular redistribution charges during excitation affects intramolecular hydrogen bond strength.

ISSN: 2472-3703 DOI: 10.6911/WSRJ.202506_11(6).0010

Table 2. Major orbital leaps and corresponding contributions (%)

Compounds	Transition	Component	CI
o-HBT-H	$S_0 \rightarrow S_1$	HOMO→LUMO	96.2%
m-HBT-H	$S_0 \rightarrow S_1$	HOMO→LUMO	97.4%

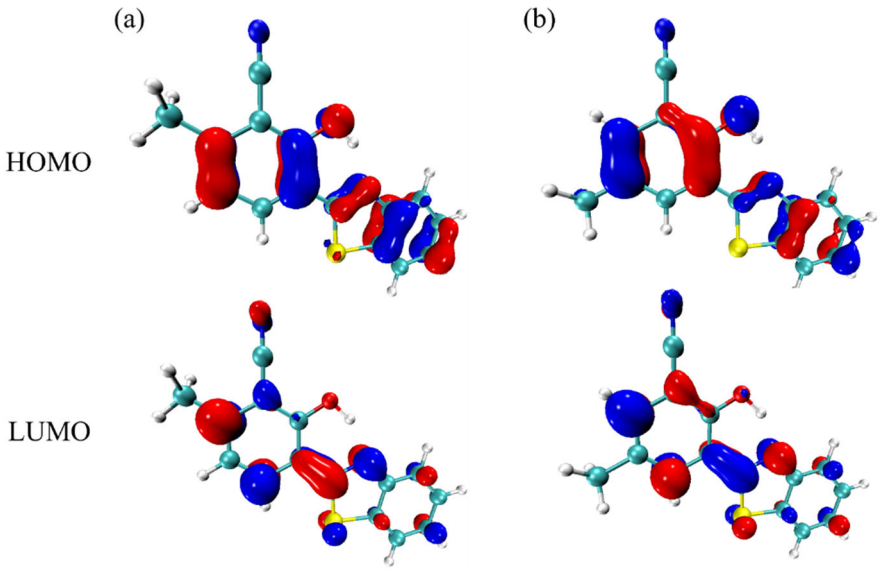

Figure 4. Molecular configurations of o-HBT-H (a), m-HBT-H (b) in S_0 (left), S_1 (right) state

Table 3. Mulliken charge (a.u.) distribution on O1 and N1 of o-HBT-H and m-HBT-H

	O_1		N_1	
	S_0	S_1	S_0	S_1
o-HBT-H	-0.266	-0.261	-0.125	-0.135
m-HBT-H	-0.270	-0.268	-0.127	-0.132

3.4. Non-covalent interactions analysis

A comprehensive investigation into electron density and its interaction region indicator (IRI) [16, 17] isosurfaces can accurately express the various types of interactions with their possessed strengths. IRI scatter plot shows function value obtained by multiplying $\rho(r)$ and sign λ_2, which can reveal location, intensity and type of weak interaction. Related formulas are as follows:

$$IRI = \frac{|\Delta\rho(r)|}{[\rho(r)]^a} \tag{1}$$

$$\Omega(r) = sign(\lambda_2)\rho(r) \tag{2}$$

As shown in Fig. 5, red, green and blue represent nonbond repulsive interaction, van der Waals interactions and hydrogen bond interaction, respectively. During excitation process, hydrogen bond properties of two isomers, o-HBT-H and m-HBT-H, demonstrate significant disparities. As demonstrated in Fig. 5, hydrogen bond characteristic peaks of o-HBT-H and m-HBT-H in S_0 state are located at -0.054 and -0.055, respectively. Upon excitation of system to S_1 state, a significant left shift is observed in hydrogen bond characteristic peaks for both

ISSN: 2472-3703 DOI: 10.6911/WSRJ.202506_11(6).0010

molecules. The peak position of o-HBT-H shifts to -0.066, while m-HBT-H exhibits a much more pronounced left shift, with its peak position moves to -0.078.

The leftward shift of characteristic peaks in S_1 state indicates a significant increase intramolecular hydrogen bond strength. The isosurface analysis further indicates change intramolecular hydrogen bond strength. During $S_0 \rightarrow S_1$ state transition, isosurface colour between H_1 and N_1 of o-HBT-H and m-HBT-H molecules tends to deepen, indicating an enhancement in intramolecular hydrogen bond strength. Furthermore, hydrogen bond in m-HBT-H is more robust than o-HBT-H.

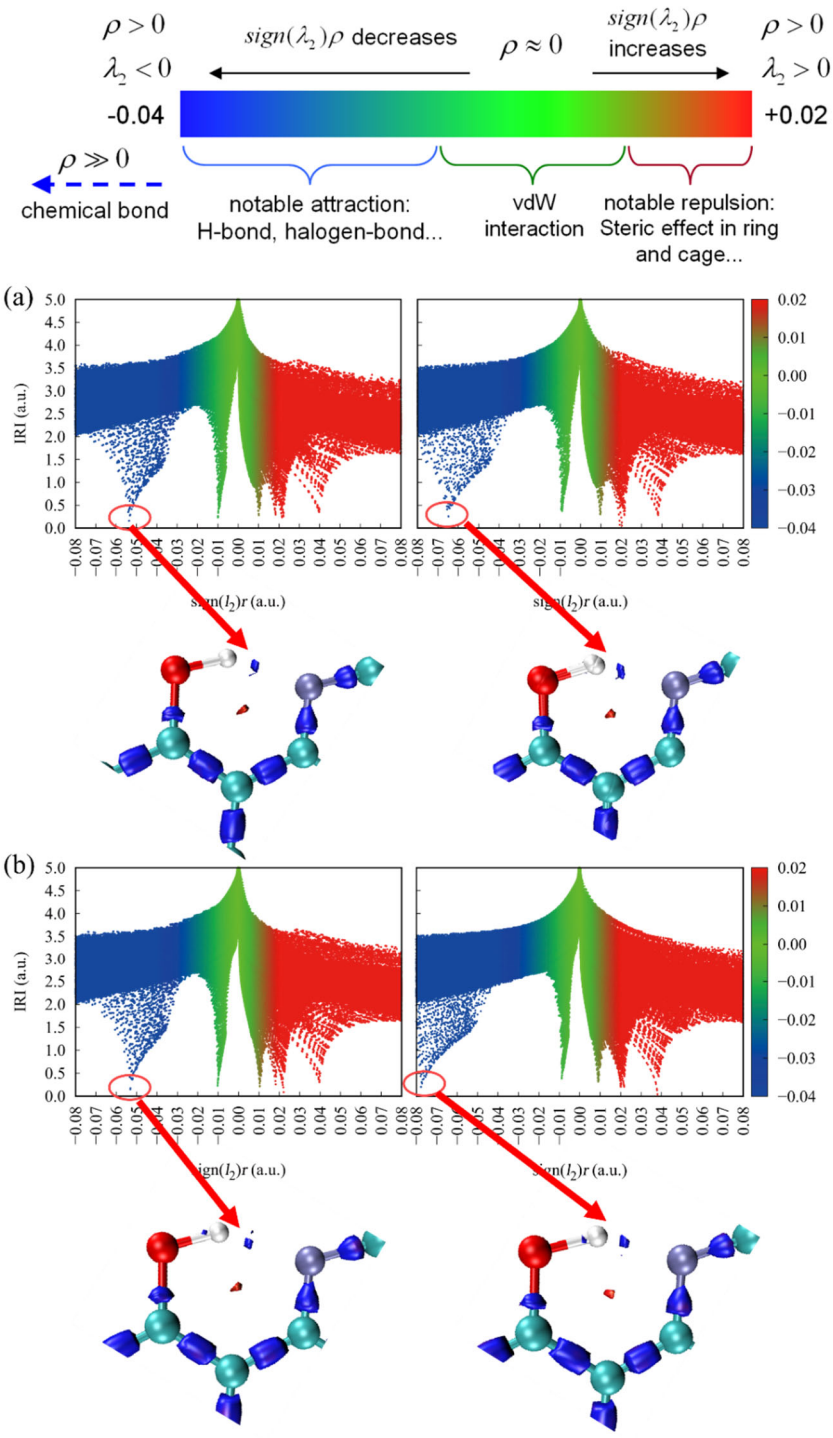

Figure 5. Scatter plots and isosurface diagrams of noncovalent interactions of o-HBT-H(a), m-HBT-H(b) in S_0 (left) and S_1 (right) state

ISSN: 2472-3703 DOI: 10.6911/WSRJ.202506_11(6).0010

3.5. IR spectrum

Changes in IR vibrational frequency is typically utilised as a criterion for determining hydrogen bond strength. Therefore, IR vibrational spectra for o-HBT-H and m-HBT-H were calculated separately, with focus being on vibrational frequencies of O_1-H_1 group associated with hydrogen bond.

The O_1-H_1 stretching vibrational peaks of o-HBT-H and m-HBT-H in S_0 state are located at 3085.10 cm^{-1} and 3105.51 cm^{-1}, respectively, and peaks in S_1 state are located at 2290.65 cm^{-1} and 2292.86 cm^{-1}, respectively. The O_1-H_1 vibrational peak of m-HBT-H in S_1 state exhibits a greater redshift compared to o-HBT-H. Result implies that intramolecular hydrogen bond is stronger in S_1 state and m-HBT-H is more prone to undergo ESIPT process.

3.6. Core application scenarios in investment management

The potential energy curves effectively illustrate proton transfer process in both S_0 and S_1 states. We calculated curves for o-HBT-H and m-HBT-H in S_0 and S_1 states, as presented in Fig. 6. In S_0 state, proton transfer potential barriers are 5.780 kcal/mol for o-HBT-H and 6.018 kcal/mol for m-HBT-H. In S_1 state, corresponding barriers are 0.772 kcal/mol for o-HBT-H and 0.080 kcal/mol for m-HBT-H. Result indicates that both isomers are more prone to proton transfer in S_1 state. Furthermore, lower potential barrier for m-HBT-H in S_1 state compared to o-HBT-H indicates that m-HBT-H is more likely to undergo ESIPT process.

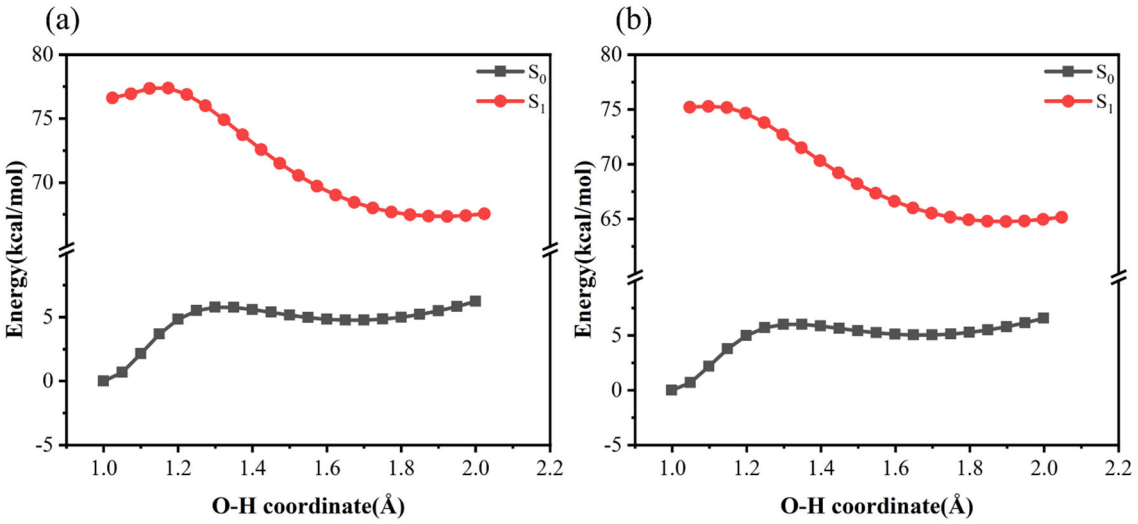

Figure 6. Potential energy curves of o-HBT-H (a) and m-HBT-H(b)

4. CONCLUSION

In conclusion, this study provides a comprehensive investigation into how methyl position affects ESIPT process in benzothiazole-based fluorescent probes. By comparing variations of major dihedral angles and bond length parameters, twisted intramolecular charge transfer was shown to occur only for m-HBT-H in S_1 state. Both molecules exhibit enhanced hydrogen bonding from S_0 to S_1 state. The result indicates that, compared to o-HBT-H, m-HBT-H exhibits greater charge transfer on O_1 atom and weaker binding to H_1 atom during excitation. The interactions between N_1 and H_1 atoms are more pronounced, and intramolecular hydrogen bond strength is enhanced in S_1 state. With a lower proton transfer barrier than o-HBT-H, m-HBT-H is more prone to ESIPT processes. Result demonstrates that methyl position markedly influences ESIPT process of HBT-H derivatives.This research offers valuable theoretical insights for designing molecules with tailored ESIPT characteristics and developing high-performance fluorescent sensors. It also deepens the understanding of the relationship between substituent

ISSN: 2472-3703 DOI: 10.6911/WSRJ.202506_11(6).0010

position and photophysical properties, providing crucial references for future studies and practical applications in this field.

REFERENCES

[1] Liao, Wenyi, Zhang, Shuwei, Wang, Xuewen, Sun, Yuyuan, Wang, Ting, Xu, Huaqian, Yuan, Yu, Chen, Gang and Jia, Xiaodong. An effective HBT/indanone-based fluorescent probe for cysteine detection in cells [J]. Dyes and Pigments, 2023, (219), 111649.

[2] Wang, Zhenkai, Yan, Miao, Yu, Miaomiao, Zhang, Gang, Fang, Weiwei and Yu, Fabiao. A Fluorescent Probe with Zwitterionic ESIPT Feature for Ratiometric Monitoring of Peroxynitrite In Vitro and In Vivo [J]. Analytical Chemistry, 2024, (96), 3600-3608.

[3] Oguz, Mehmet, Aydin, Duygu, Malkondu, Sait and Erdemir, Serkan. Specific and low-level detection of Hg2+ and CN- in aqueous solution by a new fluorescent probe: Its real sample applications including cell, soil, water, and food [J]. Sensors and Actuators B: Chemical, 2025, (433), 137527.

[4] Chen, Zhen, Zhong, Xinxin, Qu, Wangbo, Shi, Ting, Liu, Heng, He, Hanping, Zhang, Xiuhua and Wang, Shengfu. A highly selective HBT-based “turn-on” fluorescent probe for hydrazine detection and its application [J]. Tetrahedron Letters, 2017, (58), 2596-2601.

[5] Yu, Xue-fang, Xiao, Bo, Li, Qingzhong and Cheng, Jian-bo. Sensing mechanism of HBT based F anion fluorescence sensor: A theoretical study [J]. Sensors and Actuators B: Chemical, 2019, (280), 162-170.

[6] Luo, Yuehong, Chen, Kaijin, Wang, Wenhui, Bei, Ruxin, Li, Chuying, Long, Yubo, Zhou, Zhuxin, Liu, Siwei, Chi, Zhenguo, Xu, Jiarui and Zhang, Yi. Synthesis and characterization of a large Stokes-shifted fluorescent imide and its related polyimides bearing 2-(2′-hydroxyphenyl)benzothiazole moieties [J]. Journal of Materials Chemistry C, 2023, (11), 9252-9261.

[7] Erdemir, S., Aydin, D. and Oguz, M. A Ratiometric and Switchable Fluorescent Sensor Based on Calix[4]arene-HBT With a Large Stokes Shift for the Real-Time Detecting of Zn2+ and Cu2+ in Living Cells [J]. IEEE Sensors Journal, 2023, (23), 6734-6741.

[8] Zhao, Li-xia, Chen, Kun-yu, Xie, Kai-bo, Hu, Jia-jun, Deng, Meng-yu, Zou, Yue-li, Gao, Shuang, Fu, Ying and Ye, Fei. A benzothiazole-based “on-off” fluorescence probe for the specific detection of Cu2+ and its application in solution and living cells [J]. Dyes and Pigments, 2023, (210), 110943.

[9] Frisch, M. J., Trucks, G. W., Schlegel, H. B., Scuseria, G. E., Robb, M. A., Cheeseman, J. R. et al. Gaussian 16 Rev. C.01. Journal, 2016.

[10] Gara, Rayene, Morales-García, Ángel, Arfaoui, Youssef and Illas, Francesc. Density Functional Theory (DFT) and Time-Dependent DFT (TDDFT) Studies of Porphyrin Adsorption on Graphene: Insights on the Effect of Substituents and Central Metal on Adsorption Energies [J]. Journal of Computational Chemistry, 2025, (46), e27526.

[11] Zhang, Zhengyi and Fang, Hua. Regulating fluorescent properties and ESIPT behavior of novel flavone-based fluorophore by replacing oxygen atom in proton donor/acceptor with sulfur atom: A TD-DFT study [J]. Journal of Luminescence, 2024, (265), 120209.

[12] Kerdpol, Khanittha, Daengngern, Rathawat and Kungwan, Nawee. Dynamics simulation of excited-state proton transfer reactions of 8-hydroxyquinoline with water clusters: A TD-DFT study [J]. Journal of Molecular Liquids, 2023, (383), 122087.

[13] Lu, Tian and Chen, Feiwu. Multiwfn: A multifunctional wavefunction analyzer [J]. Journal of Computational Chemistry, 2012, (33), 580-592.

ISSN: 2472-3703 DOI: 10.6911/WSRJ.202506_11(6).0010

[14] Lu, Tian and Chen, Qinxue. van der Waals potential: an important complement to molecular electrostatic potential in studying intermolecular interactions [J]. Journal of Molecular Modeling, 2020, (26), 315.

[15] Humphrey, William, Dalke, Andrew and Schulten, Klaus. VMD: Visual molecular dynamics [J]. Journal of Molecular Graphics, 1996, (14), 33-38.

[16] Lu, Tian and Chen, Qinxue. Interaction Region Indicator: A Simple Real Space Function Clearly Revealing Both Chemical Bonds and Weak Interactions [J]. Chemistry–Methods, 2021, (1), 231-239.

[17] Lu, Tian and Chen, Qinxue. Visualization analysis of weak interactions in chemical systems [J]. Comprehensive computational chemistry, 2024, (2), 240.